APPLICATION

FOR

UNITED STATES LETTERS PATENT

TITLE: NON-SPHERICAL WHISPERING-GALLERY-MODE
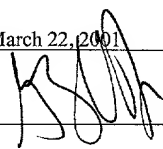   MICROCAVITY

APPLICANT: LUTFOLLAH MALEKI , XIAOTIAN S. YAO, AND
            VLADIMIR ILCHENKO

NON-SPHERICAL WHISPERING-GALLERY-MODE MICROCAVITY

This application claims the benefit of U.S. Provisional Application No. 60/191,141, filed on March 22, 2000.

Origin

5   The systems and techniques described herein were made in the performance of work under a NASA contract, and are subject to the provisions of Public Law 96-517 (35 USC 202) in which the Contractor has elected to retain title.

Background

10   This application relates to optical resonators, and more specifically, to optical whispering-gallery-mode resonators.

A dielectric sphere may be used to form an optical whispering-gallery-mode resonator which supports a special set of resonator modes known as "whispering gallery modes". These

15   modes represent optical fields confined in an interior region close to the surface of the sphere around its equator due to the total internal reflection at the sphere boundary. Microspheres with diameters on the order of $10 \sim 10^2$ microns have been used to form compact optical resonators. Such

20   resonators have a resonator dimension much larger than the wavelength of light so that the optical loss due to the finite curvature of the resonators can be small. The primary sources for optical loss include optical absorption in the dielectric

material and optical scattering due to the inhomogeneity of the sphere (e.g., irregularities on the sphere surface). As a result, a high quality factor, Q, may be achieved in such resonators. Some microspheres with sub-millimeter dimensions

5   have been demonstrated to exhibit very high quality factors for light waves, exceeding 10^9 for quartz microspheres. Hence, optical energy, once coupled into a whispering gallery mode, can circulate at or near the sphere equator with a long photon life time.

10   Whispering-gallery-mode resonators may use resonator geometries based on spheres. Since the whispering gallery modes essentially exist near the equator of a sphere, a resonator may not be necessarily a whole sphere but a portion of the sphere near the equator that is sufficiently large to

15   support the whispering gallery modes. Hence, rings, disks and other geometries formed from a proper section of a sphere may be used. Such resonators are still spherical and their whispering gallery modes are essentially identical to such modes of the respective whole spheres.

20   **Summary**

This application includes non-spherical whispering-gallery-mode resonators and their applications. In one embodiment, a spheroidal cavity is used to generate a true

finesse on the order of 10^4, a free spectral range of the order of few nanometers, and a quality-factor $Q \sim 1 \times 10^7$. Devices based on such a spheroidal cavity are also disclosed.

Brief Description of the Drawings

5   FIG. 1 shows one embodiment of a non-spherical microcavity.

FIGS. 2A, 2B, and 2C show exemplary evanescent coupling configurations for the non-spherical microcavity in FIG. 1.

FIG. 3 shows a photograph of a spheroidal cavity by

10   compressing a small sphere of low-melting silica glass between cleaved fiber tips based on the design in FIG. 1 with $D = 2a =$ 165 µm; $d = 42$ µm; and $2b = 83$ µm.

FIG. 4 shows the measured TE WG mode spectrum of the cavity shown in FIG. 2 by using a tunable DFB laser near the

15   wavelength of 1550 nm Free spectral range.

FIGS. 5A, 5B, and 5C show embodiments of opto-electronic oscillators using a spheroidal cavity as an optical delay element in a feedback loop.

FIGS. 6A and 6B show two stabilized lasers based on

20   frequency locking using a spheroidal cavity.

Detailed Description

The spheroidal microcavity geometry is designed in part

based on recognition of fundamental characteristics and

certain limitations of spherical microcavities formed from

5   partial or whole spheres. The whispering-gallery modes are

essentially closed circular waves trapped by total internal

reflection inside an axially symmetric dielectric body. The

very high quality factors Q of microspheres may be attributed

,to several factors. For example, dielectric materials for

10   microspheres are selected to have ultra-low optical loss in at

the frequencies of the supported whispering gallery modes.

Fiber-grade fused silica may be used for resonators operating

at wavelengths near 1.3 and 1.5 microns at which the optical

loss is low. For another example, the surface of the sphere

15   may be specially fabricated to minimize the size of any

surface inhomogeneities, e.g., on the order of a few Angstroms

by processes such as fire polishing. The high index contrast

in microsphere cavities is also used for steep reduction of

radiative and scattering losses with increasing radius. In

20   addition, the two-dimensional curvature of a sphere provides

for grazing reflection of all wave vector components. The

grazing incidence in a sphere can be essential for minimizing

surface scattering that would otherwise limit the Q far below

that imposed by attenuation in the material. For example, in

the integrated optical micro-ring and micro-disk cavities

based on planar waveguide technology, the light effectively

bounces from flat surfaces under *finite* angles and their

typical Q-factor is limited to 10^4 ~10^5.

5   The substantially higher Q in spheres, as compared to

micro-disks and micro-rings, comes at the price of a

relatively dense spectrum of modes. In an ideal sphere with

zero eccentricity, the optical spectrum of the sphere has

TE(TM)$_{lmq}$ modes separated by a free spectral range (FSR)

10 defined by the circumference of the sphere and related to

consecutive values of the mode index *l*. The mode index *l*

approximately represent the number of wavelengths that fit

into the optical length of the equator, *m* the number of field

maxima in the equator plane, and *q* the field maxima in the

15 direction along the radius in the equator plane.

   Each of *TE(TM)$_{lmq}$* modes, however, is degenerate and

includes (2*l*+1) modes given by the possible values of the mode

index *m*. In actual spheres, the spherical surfaces are

usually not perfectly spherical and have residual

20 nonsphericity. This deviation from the perfect spherical

surface lifts the mode degeneracy and breaks down each

TE(TM)$_{lmq}$ mode with a given value for the mode index *l* into a

series of observable *TE(TM)$_{lmq}$* modes with different values in

the mode index *m* under each value for the mode index *l*.

Therefore, a nonindeal spherical resonator exhibits two different FSRs, a "large" FSR which is the frequency spacing between two adjacent $TE(TM)_{lmq}$ modes with the same values for indices m and q but with a difference of 1 in their l values,

5   and a "small" FSR which is the frequency spacing between two adjacent $TE(TM)_{lmq}$ modes with the same l values but with a difference of 1 in their m values:

"Small" FSR:

$$v_{lmq} - v_{l,m-1,q} \sim v\frac{\varepsilon^2}{2l}$$

10   "Large" FSR:

$$v_{lmq} - v_{l-1,mq} = \frac{c}{2\pi na}(t_{lq} - t_{l-1,q}) \sim v/l$$

In silica spheres of diameter 150 to 400 micron, for example, typical fabrication techniques usually produce an eccentricity of about $\varepsilon^2 = 3\times10^{-2}$. The "large" FSR may be in

15   the range of 437 to 165GHz, or in the wavelength scale, 3.5 to 1.3nm near the center wavelength 1550nm. The "small" FSR may be in the range of 6.8 - 2.5GHz. As a result, the spheres are capable of producing a large FSR on the order of hundreds of GHz, the actual spectrum of such spheres are relatively dense

20   with a useful FSR limited by the "small" FSR typically under 10 GHz.

The above relatively dense spectrum in a typical sphere resonator may limit applications of the resonator since it can complicate spectral analysis, cause a mode hop caused by frequency jittering of a laser when such a resonator is used as a frequency reference to lock a CW laser at a selected laser frequency. In addition, intermediate filtering may be needed to eliminate some of the modes to obtain a spectrum with well-separated resonance peaks.

Hence, one way to achieve a FSR on the order of hundreds of GHz in spherical resonators without external spectral filtering is to maintain the mode degeneracy so that the "large" FSR in the whisper gallery modes $TE(TM)_{lmq}$ for given values in the mode index l can be produced in the resonator's spectrum. Under this approach, the eccentricity of the sphere should be minimized. This, however, may be technically difficult due to practical limitations of the available fabrication technologies.

In recognition of the above, the microcavities in the present application are designed to use non-spherical resonator geometries that are axially symmetric. Such a non-spherical resonator retains the two-dimensional curvature confinement, low scattering loss, and very high Q typical of microspheres, and yet approaches spectral properties of the single-mode waveguide ring. In one embodiment, instead of

minimizing the eccentricity, such a non-spherical resonator

may be formed by distorting a sphere to a non-spherical

geometry to purposely achieve a large eccentricity, e.g.,

greater than 10^{-1}. The following describes an oblate

5   spheroidal microcavity or microtorus as one example of such

non-spherical microcavities.

FIG. 1 shows one embodiment of a spheriodal microcavity

100 formed of an optical dielectric material. The cavity 100

is formed by revolving an ellipse around a symmetric axis

10   along the short elliptical axis 101. The lengths of the long

and short elliptical axes are a and b, respectively. Hence,

the eccentricity of cavity 100 is $\varepsilon^2 = (1-b^2/a^2)$. Near the

symmetry plane at the location of WG modes, toroidal surface

of outer diameter D and cross-section diameter d coincides

15   with that of the osculating oblate spheroid with large

semiaxis $a = D / 2$ and small semiaxis $b = \frac{1}{2}\sqrt{Dd}$. The dimension

D of the spheroid 100 may be less than 10 mm for operations in

the optical and microwave spectral ranges. The eccentricity

may be greater than 0.5 for

20   In operation, at least one optical coupling element may

be positioned near the cavity 100 to evanescently couple an

input beam into the cavity 100 in one or more whispering

gallery modes. An optical fiber or a planner waveguide

configured with an angle-polished facet may be used as this

optical coupling element. A microprism may also be used to

provide the proper evanescent coupling. FIGS. 2A and 2B show

the above optical coupling mechanisms. FIG. 2C shows that,

5   when two such optical coupling elements are used, one is to

couple light into the cavity 100 and the other is to couple

light out of the cavity 100.

Analysis of the spectrum of the dielectric spheroid 100

is not a trivial task, even numerically. In contrast to a

10   sphere of a small eccentricity, analysis in highly-eccentric

spheroids generally cannot be based on simple geometrical

approximations. Unlike the case of cylindrical or spherical

coordinates, orthogonal spheroidal vector harmonics that

satisfy boundary conditions may not be derived via a single

15   scalar wave function. Furthermore, the calculation of

spheroidal angular and radial functions is also a nontrivial

task.

The WG mode eigenfrequencies of the cavity 100 for a

radius a much larger than the wavelength of the a WD mode may

20   approximately represented as follows:

$$nk_{lmq}a \approx t_{lq} - \frac{\chi}{\sqrt{n^2-1}} \, ,$$ (1)

where t_{lq} is the q-th zero of the spherical Bessel function of the order l and $\chi = n$ for TE-mode and $\chi = 1/n$ for TM-mode. For large l, $t_{lq} \sim l + O(\, l^{1/3}\,)$, which may be calculated either directly or approximated via the zeroes of the Airy function.

5   See, e.g., M.Abramowitz, I.A.Stegun, eds., Handbook on mathematical functions, New-York, Dover Publ. (1970).

The meaning of small second term on the right hand side of Eq.(1) may be understood by considering the following. First, a WG mode is quasiclassically a closed circular beam supported by the total internal reflection within the cavity

10   100. Secondly, the optical field tunnels outside of the cavity 100 at the depth $1/k\sqrt{n^2 - 1}$. Thirdly, the tangential component of E (TE-mode) or the normal component of E (TM-mode) at the surface of the cavity 100 is continuous at the

15   boundary. Eigen frequencies of high-order WG modes ($l \gg 1; l \approx m$) in dielectric spheres can be approximated via solutions of the scalar wave equation with zero boundary conditions, because most of the energy is concentrated in one component of the field ($E_\square$ for TE-mode and E_r for TM-mode).

20   Based on above considerations, the WG mode eigenfrequencies can be estimated for the oblate spheroid 100 of large semiaxis a, small semiaxis b, and eccentricity $\varepsilon = \sqrt{1 - b^2/a^2}$. Since WG modes are localized in the "equatorial"

plane, the radial distribution may be approximated by

cylindrical Bessel function $J_m(n\widetilde{k}_{mq}r)$ with $n\widetilde{k}_{mq}a = na\sqrt{k_{lmq}^2 - k_\perp^2} \approx T_{mq}$,

where $J_m(T_{mq}) = 0$ and $k_\perp$ is the wavenumber for quasiclassical

solution for angular spheroidal functions and can

5 approximately written as:

$$k_\perp^2 \approx \frac{2(l-m)+1}{a^2\sqrt{1-\varepsilon^2}}m.$$

more rigorous considerations can follow the approach given in

10 I.V.Komarov, L.I.Ponomarev, S.Yu.Slavyanov, Spheroidal and

Coulomb Spheroidal Functions, Moscow, Nauka (1976). Taking

into the account that $T_{mq} \approx t_{lq} - (l - m + 1/2)$, the following

approximation can be derived:

$$nk_{lmq}a - \frac{\chi}{\sqrt{n^2-1}} \approx na\sqrt{\widetilde{k}_{mq}^2 + k_\perp^2} \approx T_{mq} + \frac{k_\perp^2 a^2}{2T_{mq}} \approx t_{lq} + \frac{2(l-m)+1}{2}(\frac{1}{\sqrt{1-\varepsilon^2}}-1)$$

(2)

For very small ε, Eq.(2) yields the same value for "small" FSR

(frequency splitting between modes with successive $m \approx 1$).

See, e.g., H.M.Lai, P.T.Leung, K.Young, P.W.Barber, S.C.Hill,

20 Phys. Rev. A 41, 5187-5198 (1990).

The results of the approximation in Eq. (2) for $l = 100$

may be compared to numerically calculated zeroes of the radial

spheroidal functions. Even with a large eccentricity of $\varepsilon =$

0.8, the deviation is no more than 5% in the estimate of m,

5 $m+1$ mode splitting and 0.1% in the absolute mode frequencies.

For larger l and smaller ε, the error should evidently be

smaller. As follows from Eq. (2), with increasing

eccentricity ε, "small" FSR - frequency interval between modes

with successive m - becomes compatible in magnitude with the

10 "large" FSR:

$$(k_{l+1mq} - k_{lmq}) \sim (k_{lm+1q} - k_{lmq}) \sim k_{lmq} / l .$$

In addition, excitation conditions for modes with different m

15 become more selective: e.g. optimal angles for prism coupling

vary with ε as $\dfrac{k_{\perp}}{k_{lmq}} \propto (1-\varepsilon^2)^{-1/4}$.

FIG. 3 shows a photograph of a spheroidal (microtorus)

cavity formed by compressing a small sphere of low-melting

silica glass between cleaved fiber tips. The combined action

20 of surface tension and axial compression resulted in the

desired spheroidal geometry. One of the fiber stems is then

cut and the whole structure is installed next to a prism

coupler for evanescent coupling as shown in FIG. 2B for measurements.

FIG. 4 shows the measured WG mode spectrum by using a tunable DFB laser near the wavelength of 1550 nm. The laser

5   was continuously frequency-scannable within the range of ~80GHz by modulating the current, and from 1545.1 to 1552.4 nm by changing the laser temperature. The spectrum with a spectral range of 900 GHz was compiled from 15 individual scans with 60GHz increments obtained by changing the

10 temperature. The frequency reference for "stitching" the spectral fragments was obtained by recording the fringes of a high-finesse ($F \sim 120$) Fabry-Perot ethalon (FSR = 30 GHz) and additional frequency marks provided by 3.75 GHz amplitude modulation. The total drift of the FP was less than 400 MHz

15 over the full 15-minute measurement time. The spectrum is reduced to only two whispering-gallery modes of selected polarization excited within the "large" free spectral range of the cavity FSR = 383 GHz, or 3.06 nm in the wavelength domain. The transmission of "parasitic" modes is at least 6dB smaller

20 than that of the principal ones. With individual mode bandwidth of 23MHz, the finesse $F = 1.7 \times 10^4$ and Q = 8.5×10^6 are therefore demonstrated with this micro-resonator.

The above measured result is comparable to the predictions of the approximate expression in Eq. (2). For a

= 82.5μm, b = 42.5μm, the eccenticity is ε = 0.86. The

refraction index of the dielectric material is n = 1.453. The

principal mode number for TE-modes at the wavelength 1550nm

should be $l \approx 473$. The "large" FSR is

5

$$v_{lmq} - v_{l-1,mq} = \frac{c}{2\pi na}(t_{lq} - t_{l-1,q}) = \frac{c}{2\pi na}(1 + 0.617l^{-2/3} + O(l^{-5/3})) \approx 402GHz,$$

and the "small" FSR is

10

$$v_{lmq} - v_{l,m-1,q} = \frac{c}{2\pi na}(\frac{1}{\sqrt{1-\varepsilon^2}} - 1) \approx 382GHz.$$

In the measured spectrum, the frequency separation between the

largest peaks 1 and 2 in FIG. 4 is equal to 383.7 ±.0.5 GHz.

It may therefore be attributed as corresponding to the small

15   FSR, in good agreement with the above estimate, if we take

into account an approximately 2% uncertainty in the

measurement (limited mainly by the precision of geometrical

evaluation of cavity dimensions). The separation between the

peaks 3 and 4 in Fig. 4, is equal to 400.3 ±. 0.5 GHz, which

20   is close to the estimate value of the "large" free spectral

range.

It may be argued that despite the large splitting between the modes with adjacent values of index m (of the order of "large" FSR), one may still expect a dense spectrum resulting from the overlap of many mode families with different

5 principal number l. In practice, however, it is exactly the coincidence in the frequency domain of WG modes with different main index l, and rapidly increasing difference $l - m$, that should be responsible for effective dephasing of the "idle" modes from the evanescent coupler, resulting in the reduction

10 of modes in the observed spectrum. In addition to increasing phase mismatch for excitation of WG modes with complex "transverse" structure ($l - m > 1$), reduced amplitude of these modes may also be the result of their lower intrinsic quality-factor. With smaller unloaded Q, critical coupling for these

15 modes would require closer position of the cavity to the excitation prism of waveguide.

The above examples and analysis indicate that a spheroidal microcavity can be designed to achieve a substantial reduction (up to 2 orders of magnitude) in the

20 number of excited WG modes in highly oblate spheroids compared to typical microspheres. This reduction in the mode density can be obtained without sacrificing the high Q associated with these structures. The novel type of optical microcavity demonstrates a true finesse on the order of 10^4, a free

~15~

spectral range of the order of few nanometers, and a quality-factor $Q \sim 1 \times 10^7$. It is contemplated that a complete elimination of "transverse" WG modes may be expected in spheroidal cavities of higher eccentricity. Further increase

5 of the Q and the finesse may also be expected with a refinement of the fabrication technique. The decrease in the density of mode spectrum of ultra-high-Q microcavities offers new applications in laser stabilization, microlasers, various passive photonics devices, and in fundamental physics

10 experiments.

FIGS. 5A, 5B, and 5C show exemplary opto-electornic oscillators that use a spheroidal microcavity as an optical delay element. Compared to previously disclosed opto-electronic oscillators with microspheres operating in the

15 microwave band (typical frequencies ~3-30GHz), the OEO based on micro-spheroidal (microtorus) resonator may operate robustly at much higher frequencies, corresponding to their mode spacing (FSR, free spectral range) in the submillimeter wave band (>300GHz) and further, in Terahertz frequency

20 domain(>1000GHz). Such an OEO may include an electrically controllable optical modulator 532 and at least one active opto-electronic feedback loop that comprises an optical part and an electrical part interconnected by a photodetector. Although many commercial electro-optical modulators cannot

operate beyond 100GHz, such an ultra-high frequency optical

modulator may be constructed on the basis of spheroidal

resonator formed of electro-optic material as described later

in this application. Modulator for the OEO needs not be

5   operated in wide range of frequencies, therefore high

efficiency can be achieved by using double microwave and

optical resonance. The opto-electronic feedback loop receives

the modulated optical output from the modulator 532 and

converted it into an electrical signal 524 to control the

10 modulator 532. The loop produces a desired delay and feeds

the electrical signal in phase to the modulator 532 to

generate and sustain both optical modulation and electrical

oscillation in the RF range when the total loop gain of the

active opto-electronic loop and any other additional feedback

15 loops exceeds the total loss.

The OEOs implement a CW signal laser 530 to produce a

signal beam at an optical carrier frequency which may be

tunable. The signal optical modulator 532 modulates the

signal beam to produce the signal 536. The signal optical

20 modulator 532 may be an amplitude modulator or a phase

modulator. The phase modulator may be preferred in some

applications because it is relatively simple to operate and

can be designed to have low optical loss and operate without

bias.

OEOs use optical modulation to produce oscillations in frequency spectral ranges that are outside the optical spectrum, such as in RF and microwave frequencies. The generated oscillating signals are tunable in frequencies and

5 can have narrow spectral linewidths and low phase noise in comparison with the signals produced by other RF and microwaves oscillators. Some examples of OEOs are disclosed in U.S. Patent Nos. 5,723,856, 5,777,778, 5,917,179, and 5,929,430, and U.S. Patent Application No. 09/491,988 filed

10 January 2000.

FIG. 5A shows a dual-loop OEO 500A in which an optical delay element 501 or 502 such as a fiber loop or the above optical spheroidal resonator is included in each opto-electronic feedback loop 510 or 520. Alternatively, one of

15 the feedback loops may be replaced with an electrical feedback loop. A RF coupler may be used to split a portion of the RF feedback signal 524 to produce an output RF signal 526. One feedback loop may be removed to form a single-loop OEO.

FIG. 5B shows a coupled OEO which directly couples a

20 laser oscillation in an optical feedback loop 530 to an electrical oscillation in an opto-electronic feedback loop 540 which includes an optical portion with an optical delay element 542 and an electrical portion that includes an optical-to-electrical conversion block 544 (e.g., a

photodetector). The optical gain of the optical feedback loop 530 is controllable by an electrical signal 524 from the opto-electronic loop 540, e.g., a semiconductor optical amplifier (SOA) 532 may be disposed in the optical loop 530. Here, the

5 optical feedback loop 530 and the SOA 532 function as the signal laser and the signal modulator 532 in FIG. 5A. A RF coupler 548 may be used to split a portion of the signal 524 as the output RF signal 526.

In addition, opto-electronic oscillators can also be

10 implemented by having at least one active opto-electronic feedback loop that generates an electrical modulation signal based on the stimulated Brillouin scattering. FIG. 5C shows such a Brillouin OEO which includes a Brillouin optical medium 560 in an opto-electronic feedback loop 562 and uses the

15 natural narrow linewidth of the Brillouin scattering to select a single oscillating mode. A pump laser 564 is used to generate a Brillouin pump beam in the Brillouin medium 560. A photodetector 566 converts the optical signal in the loop 562 into an electrical feedback signal equivalent to the RF signal

20 108. A RF coupler 548 may be used to split a portion of the detector output as the output RF signal 526.

The above spheroidal resonator operates to store optical energy only in certain whispering gallery modes. When the optical feedback caused by a round trip around the cavity has

a phase delay of $N2\pi$ (N=1, 2, 3, …), the optical resonator

operates in a resonance and optical energy accumulates inside

the resonator with a minimum loss. When the optical energy is

coupled out at this resonance condition, the output is

5   maximized. However, when the optical feedback has a phase

delay other then $N2\pi$, the amount of optical energy accumulated

in the resonator reduces from its maximum value and,

accordingly, the coupled output is also reduced from its

maximum value. Thus, the resonator can be modulated to

10   produce a modulation on the output. The modulation on the

phase delay is not limited to the phase difference between a

resonance condition and a non-resonance condition and can be

between any two different values in the phase delay. In fact,

the phase delay may be biased at a value where a change in the

15   phase delay produces the maximum change in the output energy.

The dielectric material in the spheroidal resonator may

be formed of an electro-optic material so that an external

electrical signal can be used to change the refractive index

of the resonator to change the whispering-gallery mode

20   condition and hence the output coupling. Such an optical

modulator can be designed to operate at a low operating

voltage on the millivolt level, to achieve a high modulation

speed at hundreds of gigahertz or higher, and have a compact

package. The optical coupling with the resonator may be

implemented with waveguides or fibers for integration with

other fiber optical elements or integrated electro-optical

circuits formed on substrates. Hence, such optical modulators

may be used in a variety of applications having optical

5   modulation, including optical communication and optical signal

processing.

Under proper configurations, either the spheroidal

resonator alone or the spheroidal resonator in connection with

a proper electrical strip line can form an electrical

10   resonator to support electrical energy in the same whispering

gallery modes with proper phase matching conditions. Hence,

electrical and optical waves can coexist and co-propagate in

certain whispering gallery modes. When the sphere is formed

of an electro-optic material, the electrical wave can be used

15   to alter or modulate the dielectric constant of the sphere and

hence modulate the light based on the electro-optic effects.

It is further contemplated that, the spheroidal cavity

may be formed of a laser-active material with action ions such

as rare earth ions to operate as a miniature solid-state laser

20   when a proper optical pumping scheme is provided. The laser

active material can produce an optical gain at a laser

emission wavelength by absorbing pump light at a pump

wavelength longer than the laser emission wavelength. Because

of the small volume and high Q of whispering-gallery modes,

such a laser can combine very low threshold and narrow

emission linewidth. For example, the angle-polished fiber

coupler shown in FIG. 2A may be used to couple a pump beam

into the spheroidal cavity and to couple the laser beam out of

5   the cavity, both through evanescent fields of the whispering

gallery modes.

In particular, the pump beam need be coupled into a pump

WG mode and the laser beam is generated within the cavity in a

laser WG mode. Therefore, the angle of the end facet of the

10   fiber coupler is selected to match the mode matching

conditions for both the pump and the laser beams. First, the

fiber coupler matches the mode of the pump light guided by

the fiber to a pump whispering gallery mode at the pump

wavelength in the cavity. Secondly, the fiber coupler matches

15   at least one laser whispering gallery mode at the laser

wavelength to a guided mode at the laser wavelength in the

fiber so that the output laser beam can be transmitted in the

fiber. Both the laser whispering gallery mode and the pump

whispering gallery mode spatially overlap in the cavity 130 to

20   promote efficient energy conversion from the pump wavelength

to the laser wavelength.

The above spheroidal (microtorus) resonators may also

used to stabilize the frequency and narrow the emission

linewidth of cw semiconductor diode lasers to take the

advantage of the well-separated and clean resonance peaks of

the WD modes. FIGS. 6A and 6B show two examples. Because of

very high Q of modes (~10^8 instead of ~10^2 in diode laser

cavity itself), frequency fluctuations in such a coupled

5 system can be suppressed by many order of magnitudes allowing

creation of an ultracompact laser source with sub-kHz

linewidth. This linewidth was previously achievable in

larger-size cavity solid state lasers or complex stabilized

systems based on external Fabry-Perot resonators.

10   This spherical microcavity was previously used in a

system to stabilize a diode laser in an extra-cavity

configuration. VASSILIEV VV, VELICHANSKY VL, ILCHENKO VS,

GORODETSKY ML, HOLLBERG L, YAROVISTKY AV, Narrow-line-width

diode laser with a high-Q microsphere resonator, OPT COMMUN

15 158: (1-6) 305-312 DEC 15 1998. That system, however,

suffered from the excessive density of WG modes many of which

(~100) were inside the gain bandwidth of laser diode (~several

nanometers) so that intermediate mode selectors had to be used

to suppress instabilities. With spheroidal microcavities

20 configured to have their FSR in few nanometer domain, very

simple configurations can be used as only one WG mode will

find itself in the gain maximum of the semiconductor laser.

FIG. 6A depicts the embodiment of stabilized laser based

on optical feedback provided by intracavity backscattering

~23~

effect. The output of the laser 610 is evanescently coupled into the cavity 100 as a wave 612 in a WG mode. The scattering of the wave 612 produces a counter-propagating wave 614 in a WG mode. The wave 614 is then coupled to control the frequency of the laser 610. In FIG. 6B, a laser is formed by a closed optical that includes a semiconductor optical amplifier chip 620 (in effect, a laser diode with its internal cavity totally suppressed by antireflection coating), two passive waveguide or fiber couplers 630 and 640, and a microspheroidal cavity 100. The frequency of the laser is locked at a WG mode of the cavity 100.

Although the present disclosure only includes a few embodiments, it is understood that various modifications and enhancements may be made without departing from the following claims.